RSC Advances

PAPER

View Article Online
View Journal | View Issue

Cite this: *RSC Adv.*, 2020, **10**, 31740

Development of a new bisphenol A electrochemical sensor based on a cadmium(II) porphyrin modified carbon paste electrode

Dhouha Jemmeli,[a] Chadlia Mchiri,[b] Chérif Dridi,*[a] Habib Nasri[b] and Eithne Dempsey[c]

Received 31st May 2020
Accepted 4th August 2020

DOI: 10.1039/d0ra04793g

rsc.li/rsc-advances

In this study, the (5,10,15,20-tetrakis[(4-methoxyphenyl)]porphyrinato)cadmium(II) complex ([Cd(TMPP)]) was successfully used as a modifier in a carbon paste electrode (CPE) and exploited for bisphenol A (BPA) detection. Analytical performance revealed two linear ranges from 0.0015–15 μM and 0.015–1.5 mM with a detection limit of 13.5 pM. The proposed method was implemented in water samples, which resulted in quantitative signals over the range 6.5–1000 μM with recoveries between 92.6 and 107.7% for tap water and between 96.6 to 106.0% for mineral water.

1. Introduction

Bisphenol A (BPA) is a contaminant of environmental concern and an important component in the production of plastics. It has been widely used as an additive in the production of epoxy resins and polycarbonate substances[1,2] which are widely used in food and beverage containers[3,4] due to their transparent, strong and light characteristics.[5] There is evidence that BPA can act as an endocrine disruptor, and its toxicity[6] has been widely reported in the literature, with an LD_{50} of approximately 3250 mg per kg body weight [bw] per day,[7,8] mainly based on body weight changes in two- and three-generation studies in mice and rats. Studies have shown that even low levels of BPA mimic and interfere with hormonal activity by interfering with growth and reproductive development.[9] It may be associated with several types of cancer (*e.g.* testicular, prostate, and breast cancer).[10,11] There is concern that the species can migrate from packaging into a wide range of food matrices; from water storage tanks to drinking water for instance. In addition, BPA contamination in the environment has created significant risks to ecosystems during production and recycling. Therefore, due to the harmful effects of BPA on the environment and the health of humans, it is of great importance to control its levels in environmental, biological, and food samples.[12] Hence, a rapid, specific and sensitive analytical method for BPA detection is required in the fields of environmental monitoring, food safety, and toxicity evaluation.

It is noteworthy that several analytical methods are currently used to detect BPA, including liquid chromatography-mass spectrometry, electrochemiluminescence, colorimetry, liquid chromatography coupled to UV/vis, fluorescence, enzyme-linked immunosorbent assay (ELISA) and surface-enhanced Raman scattering (SERS)[13–15] However, they have many drawbacks, all these methods need complicated pre-treatment due to requirements for the extraction and purification of the sample, they are expensive, complicated and time-consuming, thus restricting their application.[16] These methods do not allow fast processing of multiple samples and real-time detection. Therefore, researchers have turned their attention to the use of electrochemical sensors as an alternative solution for BPA quantitation due to their inherent advantages.

Electrochemical sensing lends itself to rapid on-site BPA detection at different electrode materials, including carbon[17,18] and metallic transducers.[19,20] However, electrode fouling which occurs during the electrooxidation of phenols is a challenge.[21–24] It has been found that the most common way to deal with electrode fouling problems is to modify the electrode surface with *e.g.* composite electrocatalytic materials containing nanoparticles.[24–26] As a result, a time-consuming, re-modification step (such as drop-dry or dip-coating method) is usually recommended for the regeneration of the modified electrode for every new measurement.

Carbon Paste Electrodes (CPE), which involve a coupling of pure graphite powder and liquid binder, was initially reported in 1958 by Adams,[27] and this type of electrode offers surface renewability, a stable response, high versatility, low cost, low background currents and ease of modification.[28–30] The addition of electroactive materials into the paste is advantageous and has been extensively applied in the electroanalytical community.

[a]*NANOMISENE Laboratory LR16CRMN01, Centre of Research on Microelectronics and Nanotechnology of Sousse, Technopole of Sousse, Tunisia. E-mail: cherif.dridi@crmn.rnrt.tn; Fax: +216 73823 003*

[b]*Laboratory of Physical Chemistry of Materials, University of Monastir, Faculty of Sciences of Monastir, Avenue de l'environnement, 5019 Monastir, Tunisia*

[c]*Department of Chemistry, Kathleen Lonsdale Institute for Human Health, Maynooth University, Co. Kildare, Ireland*

One of the most important roles of modifiers is to reduce the redox potential required for electrochemical reactions and to increase the sensitivity and selectivity of the assay.[31] Many materials involving metals or metal alloys, various nanotubes and nanoparticles, graphene and fullerenes, porphyrins and their derivatives, and some organic dyes have been widely used to construct electrochemical sensors.[32,33]

Amongst such materials, porphyrins and their derivatives have been used as excellent electron donors in recent years and have received extensive attention. Indeed, porphyrins are naturally occurring macrocyclic species that bind metals *via* N donor atoms on four pyrrole subunits, resulting in versatile chelating systems. Synthetic metalloporphyrins have been investigated as models for hemoproteins and enzymes such as hemoglobin, myoglobin, and cytochromes. In recent decades, researchers have extended the use of porphyrin-based compounds known as porphyrinoids (as free bases or metallated) where they are involved in several areas of chemistry, biochemistry, medicine, and physics. Actually, these applications include catalysis, photodynamic therapy, photodynamic destructions of viruses, semiconductors, nonlinear optics, photovoltaic materials, and chemical sensors.[34–36]

It is noteworthy that the cadmium ions as well as the Zinc IIB group metal are unambiguously in the +2 oxidation state in porphyrin derivatives. The direct metalation of porphyrin with zinc or cadmium leads to the tetracoordinated porphyrin species type [M^{II}(Porph)] (Porph = porphyrinato and M = Zn or Cd). The [Zn(Porph)] species are very reactive to yield pentacoordinated and hexacoordinated complexes type [Zn(Porph)(L)$_x$] (L = neutral monodentate axial ligand, $x = 1$ or 2) while [Cd(Porph)] complexes are less reactive than [Zn(porph)] and only few pentacoordinated [Cd(porph)(L)] species are reported.[37] This is the major reason why we choose this latter species for our investigation because this Cd(II) coordination compound is inert compared to other metalloporphyrins such as [Zn(Porph)]. On the other hand, very few [Cd(Porph)] complexes are reported in the literature and the only reported Cd-tetravalent porphyrin species is the [Cd(TPP)] complex where TPP is the (5,10,15,20-tetraphenyl)porphyrinato.[38] Up to date, there are no reported investigations using a tetracoordinated cadmium(II) complex with the (5,10,15,20-tetrakis)[(4-methoxyphenyl)] porphyrin (TMPP).

In this paper, a carbon paste electrode (CPE) was modified with the (5,10,15,20-tetrakis[(4-metoxyphenyl)]porphyrinato) cadmium(II), complex **[Cd(TMPP)]**, to obtain a novel electrochemical sensor CPE–**[Cd(TMPP)]** for the determination of bisphenol A (BPA). The **[Cd(TMPP)]** species were prepared and characterised by elemental analysis, FT-IR, UV/vis and ^{1}H-NMR and the prepared CPE–**[Cd(TMPP)]** electrode was characterized using cyclic voltammetry (CV). The parameters that influence the electrochemical reaction *i.e.* pH, scan rate and interferences were examined electrochemically. The prepared sensor showed two linear ranges from 1.5–15 000 nM and 0.015–1.5 mM with a 3.75×10^{-11} M limit of detection (LOD, S/N = 3). The percentage recoveries for two tested water samples (tap water and mineral water) were >92%, which shows the usefulness of this new sensor for the electrochemical detection of BPA in drinking water samples.

2. Experimental

2.1. Chemicals and apparatus

Bisphenol A (≥99.0%), Nujol oil, graphite powder (fine powder pure pH 5–6 (50 g l^{-1}, H_2O, 20 °C) and solvents were purchased from Sigma-Aldrich. All chemicals were of analytical grade and used without any further purification. Phosphate buffer was used as a supporting electrolyte and prepared with appropriate amounts of 0.1 M KCl and 0.1 M KH_2PO_4. A glassy carbon electrode (GCE) was used for electrochemical characterization studies. Working solutions were freshly prepared before use. The 5,10,15,20-tetrakis[(4-metoxyphenyl)]porphyrin) (**H_2TMPP**) was prepared according to the standard literature method.[39] The ^{1}H NMR spectra were recorded on a Bruker Advance 300 MHz spectrometer. Infrared spectra were obtained with a Shimadzu FTIR-8400 spectrophotometer in the 4000–400 cm^{-1} region. UV/Vis spectra were recorded with a WinAspect PLUS (validation for SPECORD PLUS version 4.2) scanning spectrophotometer using dichloromethane solutions in 1.0 cm path length cuvette. Mass analysis was performed by LC-MS spectrometer 2020 (Shimadzu, Japan) through electron-spray ionization (ESI) technique.

2.2. Preparation of the [Cd(TMPP)] complex

The (5,10,15,20-tetrakis[(4-metoxyphenyl)]porphyrinato)cadmium(II) (**[Cd(TMPP)]**) was synthesized according to the literature.[40] **H_2TMPP** (300 mg, 0.42 mmol) and $CdCl_2 \cdot 2H_2O$ (1 g, 1.344 mmol) were refluxed in DMF for 5 h. The color of the solution rapidly changed from purple to dark green (Scheme 1) and the reaction was monitored by UV/vis spectroscopy. The reaction mixture was then filtered, and the solvent was removed under reduced pressure to afford 0.45 g (yield ∼80%) of **[Cd(TMPP)]** as dark blue solid. CHN analysis (calculated) $C_{48}H_{36}CdN_4O_4$ (845.25 g mol^{-1}) C, 68.20; H, 4.29; N, 6.63%. Found: C, 68.36; H, 4.32; N, 6.74%. UV/vis [CH_2Cl_2: λ_{max} in nm (log ε)]: 437(4.95), 573(3.65), 617(3.66). IR [(solid, cm^{-1})]: ν(CH).: 2986–2836, ν(O–CH_3): 1246, (C=N): 1507, ν(C=C): 1601, ν(CN): 1329, δ(CCH): 999. MS-ESI (CH_2Cl_2): (m/z) = 845.5 **[Cd(TMPP)]$^+$**. ^{1}H NMR (300 MHz, $CDCl_3$, 298 K): δ(ppm) 8.86 (s, 8H, $H_{\beta\text{-pyrr.}}$), 8.14 (s, 8H, H-*ortho*), 8.11 (s, 8H, H-*meta*), 4.10 (s, 12H, O—CH_3).

2.3. Preparation of the electrodes

The CPEs were prepared according to reported procedures.[41,43,44] Graphite powder and the Nujol oil were thoroughly mixed in a 7 : 3 (w/w) ratio in a mortar to form a very fine homogeneous paste. The paste was then packed into a glass tube (2 mm diameter) with electrical contact *via* a copper wire. In the case of the modified CPE–**[Cd(TMPP)]** sensor, an optimised amount of **[Cd(TMPP)]** was added to the graphite/oil mixture and mixed to form a well dispersed and homogeneous paste.

Scheme 1 Synthesis of the [Cd(TMPP)] complex.

3. Results and discussion

3.1. Characterisation of [Cd(TMPP)]

3.1.1. UV/vis and IR spectra. Porphyrins and metalloporphyrins have a strongly conjugated π electron system. These species exhibit two π → π* electronic transitions in the visible region with a very strong B absorption band known as the Soret band, in the range 350–450 nm, with molar absorbance of about 10^5 M^{-1} cm^{-1}, and Q bands at 500–750 nm which are approximately five order of magnitude lower than the Soret band. Fig. 1 shows the spectrum of **[Cd(TMPP)]** in dichloromethane solution, with Soret band at 437 nm and Q bands at 573 and 617 nm.

The solid IR spectrum of **[Cd(TMPP)]** depicted in Fig. 2 shows absorption bands at 2986–2836 cm^{-1} attributed to *ν*(C–H) stretching frequency of the porphyrin. The C–O stretch of the OCH_3 group at the *para* positions of the phenyls of the TMPP moiety give rise to an absorption band at 1246 cm^{-1}. The bands at 1507 cm^{-1} and 1601 cm^{-1} correspond respectively to the C=C and C=N vibrations of the porphyrin while the band at 1329 cm^{-1} is attributed to the C–N stretch and the band at 999 cm^{-1} is assigned to the C–H deformation vibration of the porphyrin [*δ*(CCH)].[42]

3.1.2. ^{1}H NMR spectra. The proton NMR spectrum of the **[Cd(TMPP)]** complex is shown in Fig. 3. The phenyl protons (Ho, Ho′ and Hm, Hm′) resonate in the 7.50–8.50 ppm range and the peaks corresponding to the β-pyrrolic protons appear at 8.86 ppm. These chemical shift values are very close to those of the free base **H_2TMPP** porphyrin indicating a diamagnetic character of our Cd(II)–porphyrin derivative.[39] The absence of the peak corresponding to the N–H protons of the pyrroles, shown at −2.74 ppm for the free base porphyrin indicates the insertion of the Cd(II) cation in the cavity of the **H_2TMPP** porphyrin.

3.1.3. Cyclic voltammetry behavior of [Cd(TMPP)] at GCE. The electrochemical behavior of **[Cd(TMPP)]** was studied by CV in tetrahydrofuran (THF) solvent using tetrabutylammonium tetrafluoroborate ($(n\text{-Bu})_4NBF_4$) as supporting electrolyte (0.1

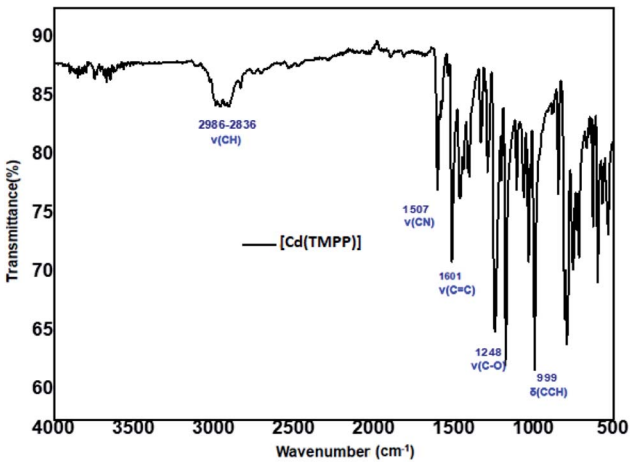

Fig. 2 Solid IR spectrum of [Cd(TMPP)] recorded in the [4000–500] cm^{-1} domain.

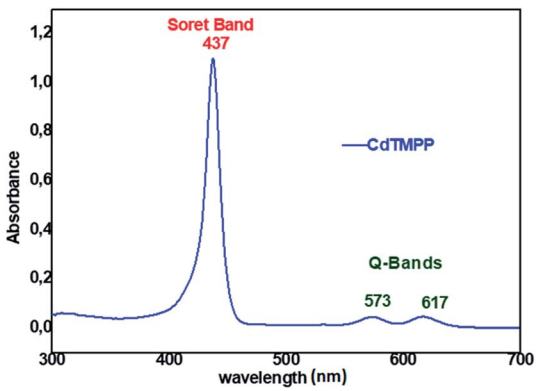

Fig. 1 UV/vis absorption spectrum of [Cd(TMPP)] with a concentration ~10^{-5} M recorded in dichloromethane.

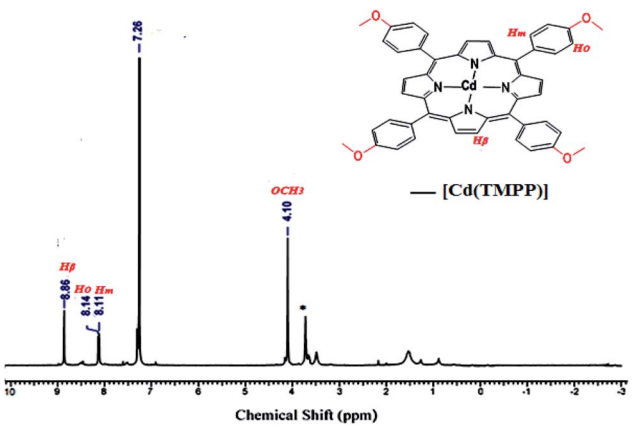

Fig. 3 ^{1}H NMR spectrum (300 MHz) of [Cd(TMPP)] recorded in $CDCl_3$.

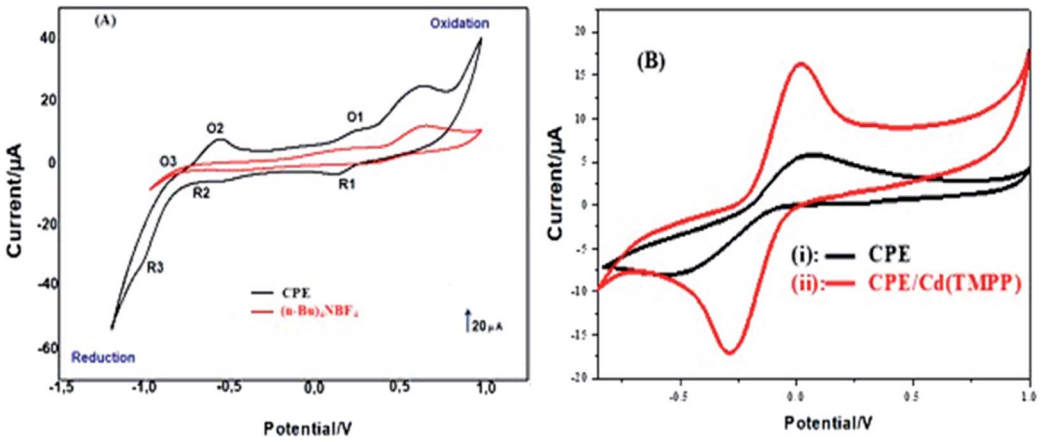

Fig. 4 (A) Cyclic voltammograms of 1 mM **[Cd(TMPP)]** (black) dissolved in THF with background electrolyte 0.1 M ($(n\text{-Bu})_4NBF_4$) (red), scan rate: 100 mVs^{-1} at a GCE with non-aqueous reference electrode. (B) cyclic voltammograms of (i) CPE and (ii) CPE–**[Cd(TMPP)]** in 5 mM $Fe(CN)_6^{3-/4-}$ solution containing 0.1 M KCl. Scan rate of 100 mVs^{-1}.

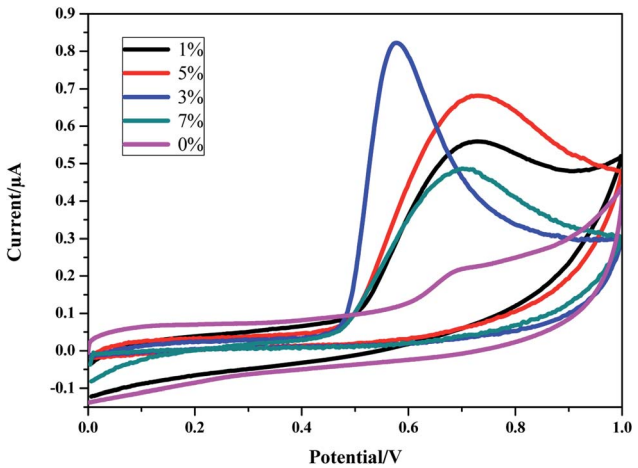

Fig. 5 Response to 1.5 mM BPA for CPE–**[Cd(TMPP)]** modified electrode over the range 0–7% w/w. Electrolyte concentration of 0.1 M phosphate buffer/20% acetonitrile (v/v) (pH 7 at 100 mV s^{-1}).

M). Fig. 4(A) presents the cyclic voltammograms of **[Cd(TMPP)]** and the background $n\text{-}Bu_4NBF_4$ supporting electrolyte recorded in THF at a glassy carbon electrode. Fig. 4(A) shows 3 oxidation waves (E_p at 0.63, 0.25 and −0.55 V *vs.* Ag/Ag^+) with corresponding cathodic processes (E_p at 0.125 V, −0.55 V and −1.0 V Ag/Ag^+), representing the central metal possibly Cd(0/II) re-oxidation at −0.55 V (O3/R3) and the π conjugated ring system of the porphyrin ligand (O1/R1, O2/R2) with contribution from methoxy electron-donating groups.[43–45].

3.1.4. Electrochemical characterisation of CPE–[Cd(TMPP)]. Fig. 4(B) shows the redox behavior of the **[Cd(TMPP)]** modified CPE using an anionic probe – $K_3[Fe(CN)_6]$ over the potential range −0.9 to 1 V *vs.* Ag/AgCl at 100 mVs^{-1}. Fig. 4(B) curve (i) shows a cyclic voltammogram at the unmodified CPE in the presence of 5 mM $K_3[Fe(CN)_6]$ resulting in a pair of well-defined voltammetric peaks with cathodic peak potential (E_{pc}) at 0.072 V and anodic peak potential (E_{pa}) at −0.286 V with peak-to-peak separation (ΔE_p) 267 mV *vs.* Ag/AgCl. Curve (ii) represents the CPE–**[Cd(TMPP)]** response in the same solution (E_{pc} of 0.019 V, E_{pa} −0.562 V ΔE_p 490 mV). Compared with the bare CPE, the peak currents of the **[Cd(TMPP)]** modified electrode decreased dramatically with increased ΔE_p indicating hindered electron transfer for the $Fe(CN)_6^{3-/4-}$ species as a result of the porphyrin modifier.

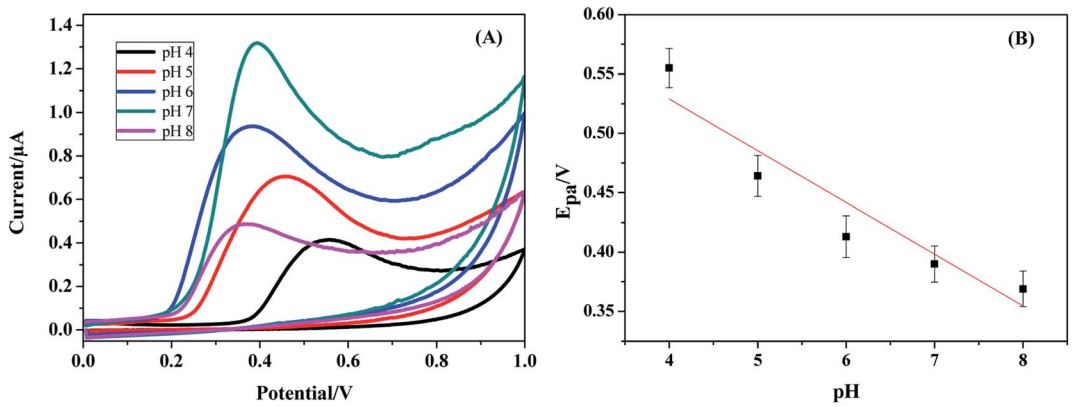

Fig. 6 (A) Cyclic voltammograms of 1.5 mM BPA at CPE–**[Cd(TMPP)]** (3% loading w/w) over pH 4–8. (B) plot of E_{pa} *vs.* pH.

3.2. Optimization of experimental conditions

3.2.1. % [Cd(TMPP)] loading in carbon paste. The purpose of this work was to fabricate a simple, low cost and a highly sensitive electrochemical sensor for the measurement of BPA. In order to obtain the best electrode configuration, different quantities of **[Cd(TMPP)]** (0–7% w/w) were added to the carbon paste electrode. The effect on the voltammetric response to 1.5 mM BPA (dissolved in 0.1 M phosphate buffer/acetonitrile 20% (v/v)) was studied. The inspection of Fig. 5 shows that the sensor response increases with an increasing amount of **[Cd(TMPP)]** modifier up to 3%. Then, the signal decreases significantly which could be due to the presence of more adsorption sites at higher % loadings leading to the accumulation of oxidation products.[46]

3.2.2. pH effect. The effect of electrolyte pH on the response of the CPE–**[Cd(TMPP)]** based sensor was studied by CV over the pH range 4–8. It was found that the intensity of the oxidation peak gradually increases with increasing pH (Fig. 6(A)) where a pH of 7 resulted in the optimal signal. The anodic peak potentials appeared to be strongly dependent on solution pH and the oxidation potential (E_{pa}) shifted negatively with increasing pH in a linear relationship indicating that protons are directly involved in the oxidation of BPA (Fig. 6(B)). This relationship obeys the following equation: $E_{pa} = -0.0586\text{pH} + 0.7648$; (correlation coefficient: $R^2 = 0.9084$). A slope of 55 mV pH^{-1}, which is close to the theoretical value of 0.0576 V pH^{-1}, clearly indicates that equal numbers of electrons and protons were involved in charge transfer.

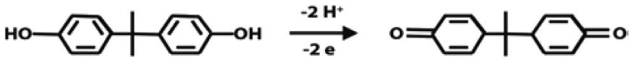

Scheme 2 Electrooxidation process of BPA at the CPE–[Cd(TMPP)].

3.2.3. Scan rate. In order to understand the electrocatalytic mechanism of BPA at the CPE–**[Cd(TMPP)]** electrochemical sensor, the effect of scan rate (v) on the oxidation current of bisphenol A was examined (Fig. 7(A)). The peak currents (I_p) increased linearly with the scan rate (v) in the [20–300] mV s^{-1} range, indicating an electrochemical process under adsorption control where the linear regression equation can be estimated by: I_{pa} (μA) = 0.061 + 0.0042 V (with a correlation coefficient $R^2 = 0.96$) (Fig. 7(B)). Meanwhile, a linear relationship between E_{pa} and ln$v$ was also observed over the 20–300 mV s^{-1} range. The equation can be expressed as: E_{pa} (V) = −0.113 ln v + 0.611 (with a correlation coefficient $R^2 = 0.9$) (Fig. 7(C)).

As for a surface controlled and totally irreversible electrode process, E_{pa} is defined by the Laviron equation:[47]

$$E_{pa} = E_o + \frac{RT}{\alpha nF}\ln\frac{RTk_o}{\alpha nF} + \frac{RT}{\alpha nF}\ln v$$

where α is the transfer coefficient, k_o is the standard rate constant of the reaction, n is the electron transfer number involved in rate determining step, v is the scan rate, E_o is the formal redox potential, R is the gas constant, T is the absolute temperature, and F is Faraday's constant. According to the linear correlation of E_{pa} *vs.* ln v, αn was found to be 1.1 from the slope of the plot. Assuming α to be 0.5,[48,49] the number of the

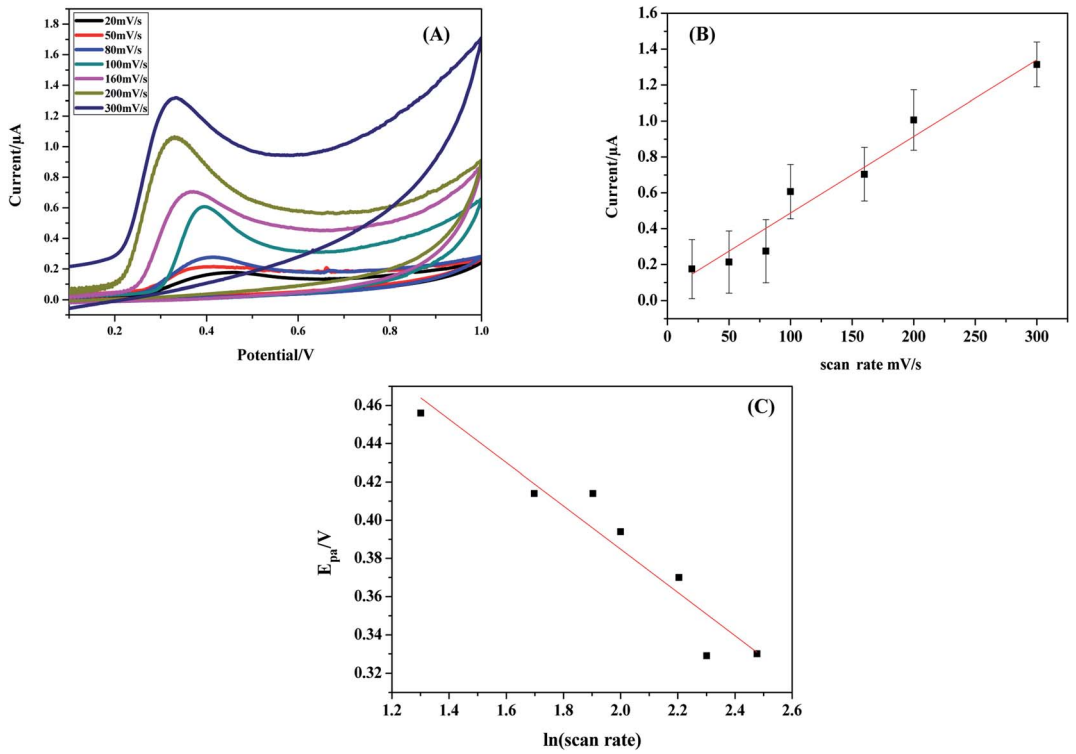

Fig. 7 (A) Cyclic voltammograms of 1.5 mM BPA at CPE–[Cd(TMPP)] over the range 20–300 mV s^{-1} (B) I_{pa} *vs.* scan rate, (C) E_{pa} *vs.* ln(scan rate).

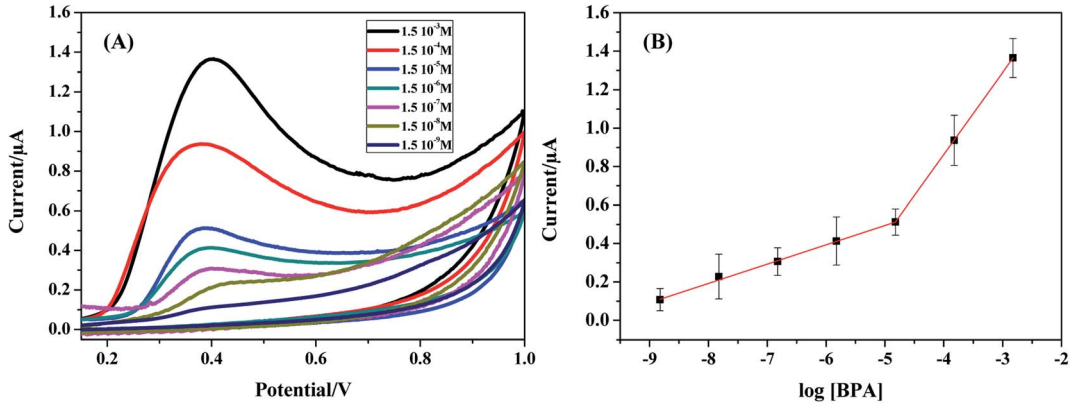

Fig. 8 (A) CV for various concentrations of BPA over the range 1.5×10^{-9} to 1.5×10^{-3} M in 0.1 M PBS (pH 7), (B) calibration plot of peak current *vs.* log[BPA].

electrons included in the electrochemical oxidation of BPA was found to be 2. According to previous reports with regards to the oxidation of BPA and other phenolic compounds and the results obtained from this work, the electrooxidation process of BPA at the modified electrode is as shown by Scheme 2. The 4 fold enhancement in current in the presence of 3% **[Cd(TMPP)]** indicates an electrocatalytic role for the porphyrin modifier. The Cd metal centre and associated redox process may play a role in accelerating the electrooxidation of the BPA molecule, making for more efficient electron and proton transfer with the associated lowering of BPA overpotential (from 0.7 to 0.6 V *vs.* Ag/AgCl). The enhancement of the available surface area results in the increase of the oxidation current and the modifier can also act to minimize surface fouling from the oxidation products.

3.2.4. Determination of the linear range and limit of detection. The analytical performance of the CPE–**[Cd(TMPP)]** sensor for BPA quantitation was tested using CV. Fig. 8(A) shows the electrochemical response of BPA oxidation as a function of BPA concentration with the corresponding calibration curve shown in Fig. 8(B). Two linear domains are visible on this curve. This behaviour has also been reported in the literature for the electroanalytical detection of BPA which was attributed to adsorption effects.[50–52] These two linear regions covered the concentration ranges of 0.0015–15 μM and 0.015–1.5 mM according to the two equations: I_{pa} (A) = 1.005 10^{-7} log[BPA] + 9.97 10^{-7} (with a correlation coefficient $R^2 = 0.998$) and I_{pa} (A) = 4.263×10^{-7} log[BPA] + 2.56 10^{-7} (with a correlation coefficient $R^2 = 0.997$) respectively. The detection limit (LOD) calculated by the formula: [(3 × Standard deviation of low concentration)/slope of the calibration curve][53] was 1.35 10^{-11} M. This value is one of the lowest LODs obtained so far in comparison with recent reported BPA sensors literature values (Table 1).

3.2.5. Interference study. The selectivity of the electrochemical sensor was also examined in phosphate buffer (pH = 7). Some phenolic species and common inorganic ions have been tested to check their levels of interference in BPA determination in the presence of 1.5 μM BPA (Table 2). In addition, inorganic ions, such as Ca^+, K^+, Zn^{2+} and Na^+ at 100-fold concentrations were shown to have no influence on BPA signals.

Table 1 Comparison of the prepared sensor for BPA detection with other reported sensors

Electrodes	Linear range (M)	LOD[a] (M)	Ref.
CTAB–CPE[b]	2.5×10^{-8} to 1.10×10^{-6}	7.5×10^{-9}	54
CoPc–CPE[c]	8.75×10^{-8} to 1.25×10^{-5}	1.1×10^{-9}	55
Thionine/CPE	0.15×10^{-6} to 45×10^{-6}	1.5×10^{-7}	56
Ordered mesoporous silica (SBA–MIP)/CPE[d]	1.0×10^{-7} to 5.0×10^{-4}	3.2×10^{-7}	57
Magnetic molecularly imprinted nanoparticles-surfactant modified/CPE	6.0×10^{-7} to 1.0×10^{-4}	1.0×10^{-7}	58
MCM-41/CPE[e]	0.22×10^{-6} to 8.8×10^{-6}	38×10^{-9}	59
ILs–GO/CPE[f]	0.09×10^{-6} to 250×10^{-6}	55×10^{-9}	60
nAg–PVP/CPE[g]	4×10^{-8} to 1.0×10^{-6}	2.5×10^{-8}	61
MWCNTox–MCPE[h]	3.0×10^{-7} to 2.1×10^{-5} and 2.4×10^{-5} to 1.0×10^{-4}	40.4×10^{-9}	62
[Cd(TMPP)]/CPE	1.5×10^{-5} to 1.5×10^{-9}	1.35×10^{-11}	This work

[a] LOD = limit of detection. [b] CTAB = cetrimonium bromide. [c] CoPc = cobalt phthalocyanine. [d] SBA–MIP = mesoporous silica–molecularly imprinted polymers. [e] MCM-41 = mesoporous silica molecular sieves. [f] ILs–GO = ionic liquids–graphene oxide. [g] nAg–PVP = silver nanoparticles–polyvinylpyrrolidone. [h] MWCNTox = oxidized multi-walled carbon nanotube.

Table 2 Influence of interferents, 100/50-fold concentration on the electrode response of 1.5 μM BPA at 0.42 V *vs.* Ag/AgCl

	Interferents	Peak change (%)
50-Fold	Hydroquinoe	−3.28
	Phenol	+2.54
	4-Octylphenol	+4.89
	Pyrocatechol	−3.78
	Dopamine	+2.96
	Ascorbic acid	+2.15
100-Fold	Ca^{+}	−4.52
	K^{+}	−1.56
	Zn^{2+}	−3.12
	Na^{+}	−3.21

Table 3 BPA detection in real drinking water samples

Sample	Added (M)	Found (M)	Recovery%	RSD% ($n = 3$)
Tap water	1.5×10^{-3}	1.39×10^{-3}	92.6	1.24
	1.5×10^{-4}	1.61×10^{-4}	107.7	2.35
	1.5×10^{-5}	1.52×10^{-5}	101.5	3.52
	1.5×10^{-6}	1.47×10^{-6}	98.3	2.82
	1.5×10^{-7}	1.46×10^{-7}	97.5	1.09
Mineral water	1.5×10^{-3}	1.45×10^{-3}	96.6	1.34
	1.5×10^{-4}	1.56×10^{-4}	104	2.11
	1.5×10^{-5}	1.49×10^{-5}	99.3	1.65
	1.5×10^{-6}	1.57×10^{-6}	104.6	1.9
	1.5×10^{-7}	1.55×10^{-7}	103.3	1.56
	1.5×10^{-8}	1.59×10^{-8}	106	1.15

These results indicated that CPE–**[Cd(TMPP)]** electrode exhibits selective reactivity to BPA in the presence of these ionic species.

3.3. Real sample analysis

In order to confirm the sensitivity and applicability of the proposed method, the fabricated **[Cd(TMPP)]**/CPE sensor was used to determine BPA in water samples (tap and mineral water). Under the optimized conditions, a known-amount of the sample was added into pH 7 phosphate buffer and then analyzed according to the above-described procedures. No BPA species were detected in the water samples (Table 3). The same samples were then spiked with different amounts of BPA and the recoveries were in the range 92.6–107.7% and 96.6–106% for tap and mineral water respectively, indicating that the sensor is perfectly adequate for application in natural samples.

4. Conclusions

This article reports the fabrication of a simple, cost-effective, and highly sensitive sensor for BPA based on a carbon paste matrix encapsulating a new cadmium(II) porphyrin derivative. The synthesis, the UV/vis, IR and proton NMR characterisation of the (5,10,15,20-tetrakis[(4-metoxyphenyl)]porphyrin)cadmium(II) complex (**[Cd(TMPP)]**) was reported. The use of the porphyrin compound as a modifier in a carbon paste electrode improved the analytical performance compared to that exhibited by glassy carbon modified with other nanomaterials. The results show that the bisphenol A oxidation signal was enhanced ad the modified electrode proved to be highly sensitive, with acceptable stability. Two linear ranges were observed from 0.0015–15 μM and 0.015–1.5 mM with a detection limit of 13.5 pM. Quantitation of BPA was enabled at this surface and analytical performance was excellent in spiked drinking water samples.

Conflicts of interest

There are no conflicts of interest to declare.

Acknowledgements

This work was supported by the Tunisian Ministry of Higher Education and Scientific Research.

References

1 A. Bhatnagar and I. Anastopoulos, *Chemosphere*, 2017, **168**, 885–902.
2 J. I. Kwak, J. Moon, D. Kim, R. Cui and Y.-J. An, *J. Hazard. Mater.*, 2018, **344**, 390–397.
3 L. A. Goulart, R. Gonçalves, A. A. Correa, E. C. Pereira and L. H. Mascaro, *Microchim. Acta*, 2017, **188**, 1–9.
4 X. Zhu, G. Wu, Y. Xing, C. Wang, X. Yuan and B. Li, *J. Hazard. Mater.*, 2020, **381**, 120908.
5 H. Filik and A. A. Avan, *Curr. Anal. Chem.*, 2017, **13**, 464–473.
6 H. Li, W. Wang, Q. Lv, G. Xi, H. Bai and Q. Zhang, *Electrochem. Commun.*, 2016, **68**, 104–107.
7 R. E. Chapin, J. Adams, K. Boekelheide, L. E. Gray Jr, S. W. Hayward, P. S. Lee, B. S. McIntyre, K. M. Portier, T. M. Schnorr, S. G. Selevan, J. G. Vandenbergh and S. R. Woskie, *Birth Defects Res., B*, 2008, **83**, 157–395.
8 L. N. Vandenberg, M. V. Maffini, C. Sonnenschein, B. S. Rubin and A. M. Soto, *Endocr. Rev.*, 2009, **30**, 75–95.
9 Y. Qiao, J. Li, H. Li, H. Fang, D. Fan and W. Wang, *Biosens. Bioelectron.*, 2016, **86**, 315–324.
10 W. Wang, X. Wang, J. Xing, Q. Gong, H. Wang, J. Wang, Z. Chen, Y. Ai and X. Wang, *Environ. Sci. Nano.*, 2019, **6**, 809–819.
11 N. J. Cabaton, P. R. Wadia, B. S. Rubin, D. Zalko, C. M. Schaeberle, M. H. Askenase, J. L. Gadbois, A. P. Tharp, G. S. Whitt, C. Sonnenschein and A. M. Soto, *Environ. Health Perspect.*, 2011, **119**, 547–552.
12 N. Caballero-Casero, L. Lunar and S. Rubio, *Anal. Chim. Acta*, 2016, **908**, 22–53.
13 E. Ferrer, E. Santoni, S. Vittori, G. Font, J. Mañes and G. Sagratini, *Food Chem.*, 2011, **126**, 360–367.
14 E. Chung, J. Jeon, J. Yu, C. Lee and J. Choo, *Biosens. Bioelectron.*, 2015, **64**, 560–565.
15 C. Peng, N. Pan, Z. Xie, L. Liu, J. Xiang and C. Liu, *Anal. Lett.*, 2016, **49**, 1492–1501.

16 K. V. Ragavan, N. K. Rastogi and M. S. Thakur, *Trends Anal. Chem.*, 2013, **52**, 248–260.
17 X. Niu, W. Yang, G. Wang, J. Ren, H. Guo and J. Gao, *Electrochim. Acta*, 2013, **98**, 167–175.
18 Y. Li, H. Wang, B. Yan and H. Zhang, *J. Electroanal. Chem.*, 2017, **805**, 39–46.
19 K. Shim, J. Kim, M. Shahabuddin, Y. Yamauchi, Md. S. A. Hossain and J. H. Kim, *Sens. Actuator B. Chem.*, 2018, **255**, 2800–2808.
20 J. Yang, S.-E. Kim, M. Cho, I.-K. Yoo, W.-S. Choe and Y. Lee, *Biosens. Bioelectron.*, 2014, **61**, 38–44.
21 A. Ghanam, A. A. Lahcen and A. Amine, *J. Electroanal. Chem.*, 2017, **789**, 58–66.
22 M. Masikini, T. T. Waryo, P. G. L. Baker, L. V. Ngqongwa, A. R. Williams and E. I. Iwuoha, *Anal. Lett.*, 2011, **44**, 2047–2060.
23 S. Poorahong, C. Thammakhet, P. Thavarungkul, W. Limbut, A. Numnuam and P. Kanatharana, *Microchim. Acta*, 2012, **176**, 91–99.
24 Z. Zheng, Y. Du, Z. Wang, Q. Feng and C. Wang, *Analyst*, 2013, **138**, 693–701.
25 J. Zhang, X. Xu and Z. Chen, *Ionics*, 2018, **24**, 2123–2134.
26 R. Wannapob, P. Thavarungkul, S. Dawan, A. Numnuam, W. Limbut and P. Kanatharana, *Electroanalysis*, 2016, **28**, 1–10.
27 R. N. Adams, *Anal. Chem.*, 1958, **30**, 1576.
28 F. Hosseini, M. Ebrahimi and H. Karimi-Maleh, *Int. J. Electrochem. Sci.*, 2018, **13**, 4923–4932.
29 N. Soltani, N. Tavakkoli, Z. S. Mosavimanesh and F. Davar, *C. R. Chim.*, 2018, **21**, 54–60.
30 M. Kumar, B. E. K. Swamy, M. H. M. Asif and C. C. Viswanath, *Appl. Surf. Sci.*, 2017, **399**, 411–419.
31 S. Shahrokhian, A. Hamzehloei, A. Thaghani and S. R. Mousavi, *Electroanalysis*, 2004, **16**, 915–921.
32 Y. X. Lin, Q. Zhou, Y. P. Lin, D. P. Tang, R. Niessner and D. Knopp, *Anal. Chem.*, 2015, **87**, 8531–8540.
33 M. Cui, J. D. Huang, Y. Wang, Y. M. Wu and X. L. Luo, *Biosens. Bioelectron.*, 2015, **68**, 563–569.
34 Z.-B. Liu, Y.-F. Xu, X.-Y. Zhang, X.-L. Zhang, Y.-S. Chen and J.-G. Tian, *J. Phys. Chem., B*, 2009, **113**, 9681–9686.
35 Z. L. Dunn, M. A. Hammer, B. J. Topham and T. M. Perrine, *J. Phys. Chem., C*, 2017, **121**, 12018–12024.
36 S. Ishihara, J. Labuta, W. V. Rossom, D. Ishikawa, K. Minami, J. P. Hill and K. Ariga, *Phys. Chem. Chem. Phys.*, 2014, **16**, 9713–9746.
37 H. Toumi, N. Amiri, M. S. Belkhiria, J.-C. Daran and H. Nasri, *Acta Crystallogr., Sect. E: Struct. Rep. Online*, 2012, **68**, 1557–1558.
38 M. P. Byrn, C. J. Curtis, I. Goldberg, Y. Hsiou, S. I. Khan, P. A. Sawin, S. K. Tendick and C. E. Strouse, *J. Am. Chem. Soc.*, 1991, **113**, 6549–6557.
39 P. F. Rodesiler, E. A. H. Griffith, N. G. Charles, L. Lebioda and E. L. Amma, *Inorg. Chem.*, 1985, **24**, 4595–4600.
40 X. Yu, Y. Chen, L. Chang, L. Zhou, F. Tang and X. Wu, *Sens. Actuator B. Chem.*, 2013, **186**, 648–656.
41 L. Ben Haj Hassen, K. Ezzayani, Y. Rousselin, C. Stern, H. Nasri and C. E. Schulz, *J. Mol. Struct.*, 2016, **1110**, 138–142.
42 C. Mchiri, S. Dhifaoui, K. Ezzayani, M. Guergueb, T. Roisnel, F. Loiseauc and H. Nasri, *Polyhedron*, 2019, **171**, 10–19.
43 G. Simonneaux, V. Schunemann, C. Morice, L. Carel, L. Toupet, H. Winkler, A. X. Trautwein and F. A. Walker, *J. Am. Chem. Soc.*, 2000, **122**, 4366–4377.
44 A. Ghosh, I. Halvorsen, H. J. Nilsen, E. Steene, T. Wondimagegn, R. Lie, E. Van Caemelbecke, N. Guo, Z. Ou and K. M. Kaddish, *J. Phys. Chem., B*, 2001, **105**, 8120–8124.
45 T. H Phan and K. Wandelt, *J. Chem. Phys.*, 2015, **142**, 101917–101925.
46 M. Siswana, K. I. Ozoemena and T. Nyokong, *Talanta*, 2006, **69**, 1136–1142.
47 E. Laviron, *J. Electroanal. Chem. Interfacial Electrochem.*, 1974, **52**, 355–393.
48 Y. Gao, Y. Cao, D. Yang, X. Luo, Y. Tang and H. Li, *J. Hazard. Mater.*, 2012, **199**, 111–118.
49 T. Zhan, Y. Song, X. Li and W. Hou, *Mater. Sci. Eng., C*, 2016, **64**, 354–361.
50 Y. Li, Y. Gao, Y. Cao and H. Li, *Sens. Actuators, B*, 2012, **171–172**, 726–733.
51 C. Hou, W. Tang, C. Zhang, Y. Wang and N. Zhu, *Electrochim. Acta*, 2014, **144**, 324–331.
52 N. Ben Messaoud, M. E. Ghica, C. Dridi, M. B. Ali and C. M. Brett, *Sens. Actuators, B*, 2017, **253**, 513–522.
53 A. Shrivastava and V. B. Gupta, *Chron. Young Sci.*, 2011, **2**, 21–25.
54 W. Huang, *Bull. Korean Chem. Soc.*, 2005, **26**, 1560–1564.
55 Y. Zhang, L. T. Wang, D. B. Lu, X. Z. Shi, C. M. Wang and X. J. Duan, *Electrochim. Acta*, 2012, **80**, 77–83.
56 M. Portaccio, D. D. Tuoro, F. Arduini, M. Lepore, D. G. Mita, N. Diano, L. Mita and D. Moscone, *Biosens. Bioelectron.*, 2010, **25**, 2003–2008.
57 Y. Wang, Y. Yang, L. Xu and J. Zhang, *Electrochim. Acta*, 2011, **56**, 2105–2109.
58 L. Zhu, Y. Cao and G. Cao, *Biosens. Bioelectron.*, 2014, **54**, 258–261.
59 F. Wang, J. Yang and K. Wu, *Anal. Chim. Acta*, 2009, **638**, 23–28.
60 H. Beitollahi and S. Tajik, *Environ. Monit. Assess.*, 2015, **187**, 257–267.
61 F. Ianesko, C. A. de Lima, C. Antoniazzi, E. R. Santana, J. V. Piovesan, A. Spinelli, A. Galli and E. Guimarães de Castro, *Electroanalysis*, 2018, **30**, 1946–1955.
62 J. Srinivas, R. J. Mascarenhas, O. D'Souza, A. K. Satpati and Z. Mekhalif, *Anal. Chem. Lett.*, 2017, **7**, 52–64.